Ultrafast field dynamics following high-intensity laser interactions with metallic wires

K. Quinn, L. Romagnani, P. A. Wilson, B. Ramakrishna and M. Borghesi
Centre for Plasma Physics, Queen's University Belfast, Belfast, BT7 1NN, UK

M. M. Notley and R. J. Clarke
Central Laser Facility, STFC, Rutherford Appleton Laboratory, HSIC, Didcot, Oxon OX11 0QX, UK

Contact | kquinn09@qub.ac.uk

L. Lancia and J. Fuchs
LULI, École Polytechnique-Université Paris VI, 91128 Palaiseau, France

A. Pipahl and O. Willi
Heinrich-Heine-Universität, 40225 Düsseldorf, Germany

R. G. Evans
Plasma Physics Group, Imperial College London, London SW7 2AZ, UK

Introduction

In the interaction of a high intensity, short pulse laser with a metallic surface, electrons are accelerated away from the focal region via a number of mechanisms. Some electrons may be lost to vacuum, leading to the build-up of a large positive electrostatic charge on the target, whilst other electrons will proceed to move in and around the region of the target via a number of processes.

An understanding of and ability to control these electron transport processes is of relevance to both the fast ignitor concept for Inertial Confinement Fusion [1] and to the mechanisms for laser-driven ion acceleration [2]. In the present research, the fields set up by laser-matter interactions enable the use of proton imaging in diagnosing the processes at work in this problem.

Proton imaging

The acceleration of multi-MeV proton beams from the rear surface of metallic foils irradiated with intense laser radiation is now generally accepted to occur via the Target Normal Sheath Acceleration mechanism [3]. The extraordinary properties of laser-driven proton beams (collimation, laminarity, short burst duration) have led to a great deal of interest as to their potential usefulness in a diverse range of applications [4], including, as is applicable to the research presented in this report, the techniques of proton imaging and deflectometry [5] which enable laser-matter interactions to be diagnosed with high spatial (μm), unparalleled temporal (ps) resolution.

The use of Radiochromic Film (RCF) [6] as a proton beam detector has become common in diagnosing the processes occurring in intense laser-matter interactions. RCF is an absolutely-calibrated dosimetry medium which turns from clear to blue on exposure to ionising radiation. Employing RCF in multi-layered stacks transverse to the incident proton beam enables the computation of information on the energy spectrum of the beam. More energetic protons will burrow to deeper films in the pack, depositing the bulk of their energy in the region around the Bragg peak, so that each layer can be assigned an effective proton energy, E_p.

In terms of the proton imaging technique, the combination of the broadband nature of laser-driven proton beams and the spectral information provided by RCF stacks provides an ingenius way of providing temporally-resolved information on an interaction. The proton beam can be well-approximated as having a point-like source. If the source-plasma distance is d and the source-detector distance is D, then the magnification of the target region at the detector will be given by $M = D/d$. The time at which a proton of energy E_p passes the target plasma, meanwhile, is given by $t_{probe} = d\,(m_p/2E_p)^{1/2}$. In this way, the multi-frame capability of the RCF stack in monitoring an interaction is exploited.

The trajectories of protons passing through regions of substantial electric and magnetic fields will be modified by the action of the Lorentz force. Hence, proton density modulations at the detector can be used to infer the magnitude and direction of the E- and B-fields present at the interaction region.

Experiment

The experiment was carried out on the Petawatt arm of the Vulcan laser [7]. Operating in dual-beam mode, 5% of the laser energy was diverted inside the target chamber to provide the interaction pulse (CPA_2), whilst the remainder provided the proton acceleration pulse (CPA_1). Typical cutoff energies of 40 MeV were observed in the probe proton beam so that the interaction could be observed over a 100 ps time window with ps resolution. Note that both the spatial and temporal resolution of the proton imaging technique will improve as energy increases – with increasing velocity, probe protons will suffer smaller deflections and be in the region of the target for shorter times.

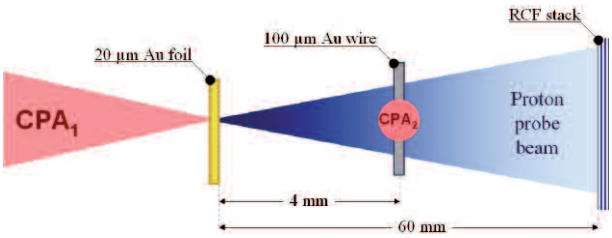

Figure 1. Experimental setup.

Observation of charge-discharge cycle

The interaction of the intense (2×10^{19} W cm^{-2} μm^{-2}) short pulse (700 fs) CPA_2 beam with a 100 μm diameter gold wire was studied.

To provide a complete temporal picture of the interaction, CPA_2 was optically delayed so as to strike the target at a time at which the region around the wire was completely enveloped in the probe proton beam. Prior to the interaction, the wire shadow can be seen in the RCF images as a central vertical band of proton depletion (a *white* region, see figure 2). The proton density at the detector, n_p, on each side of the wire image is roughly uniform, decaying only at the edges of the image where the probe beam itself becomes weaker. Some blurring between the blue (high n_p) and white (low n_p) areas can be attributed to scattering of the probe protons inside the wire. After the interaction, modulations in the proton density are witnessed. In particular, there is a pile-up of protons at some distance from the surface of the wire image, visible as a dark blue vertical band. Physically speaking, this is due to the fact that the trajectories of the protons travelling close to the wire have been modified by the action of the Lorentz force induced by the fields set up around the wire by the CPA_2 interaction.

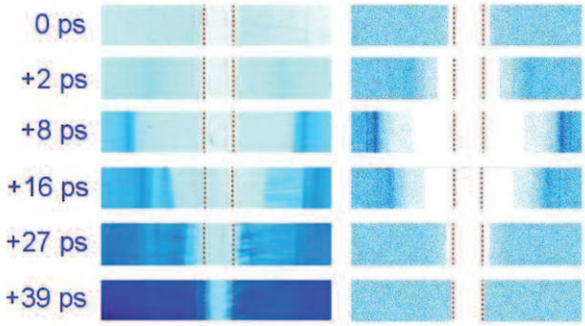

Figure 2. Experimental (left) and simulated (right) data describing wire charge-discharge cycle. The dotted red lines indicate the position of the wire. The times shown are relative to the arrival of the interaction pulse, CPA_2.

3D particle tracing simulations were used to infer the fields present around the wire. The assumption was made that the wire charging was caused by the expulsion of electrons from the focus of the laser, leaving the wire itself with a net positive charge, and an E-field directed radially outwards. The decay of this E-field with time is evident from the experimental data in that, at late times after the interaction, the probe protons remain largely undeflected. From the Ampère-Maxwell equation, the presence of such a transient E-field would be expected to produce an associated azimuthal B-field. From this starting point, a trial-and-error process was undertaken to determine the field configurations which led to the closest agreement between the simulated and experimental behaviour of $\boldsymbol{n}_p$.

The domain of variables ($\boldsymbol{r}$, $\boldsymbol{E}(\boldsymbol{r})$, $\boldsymbol{B}(\boldsymbol{r})$, $\boldsymbol{n}_p$) was explored, where $\boldsymbol{r}$ gives the radial displacement from the wire centre. The simulations indicated that, in this configuration, the experimental behaviour of $\boldsymbol{n}_p$ can only be recreated if the maximum azimuthal magnetic field strength is limited to 1 MG or below. For this experimental configuration of side-on imaging at least, the E-field appears to be dominant in producing the observed proton deflection pattern.

A best match between the experimental and simulated proton density distributions was obtained when a 1/*r*-like radial electric field profile was used in the particle tracer. The peak E-field strength required to produce the observed maximum deflection was hence determined to be ~3×10^{10} V m^{-1}.

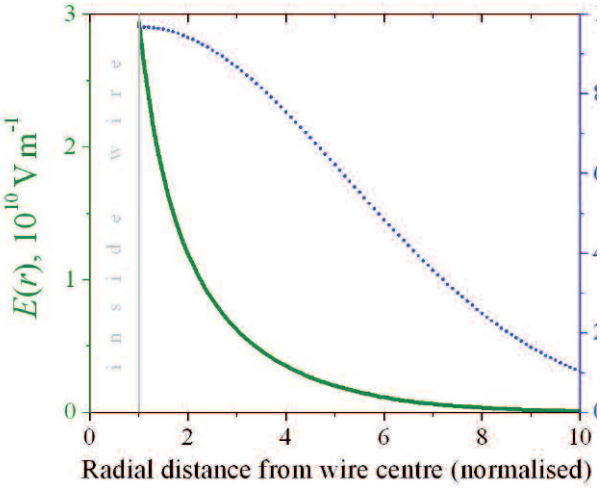

Figure 3. Radial electric field function (green) and corresponding electron density function (dotted blue) required to produce experimentally-observed proton deflection pattern. The radial electron density function, $n_e(r)$, was calculated with Poisson's equation under the assumption that the total amount of negative charge outside the wire was balanced by an equal amount of positive charge inside the wire.

As mentioned previously, temporal information is provided by RCF data due to the broadband nature of the proton beam and the fact that protons of different energies will pass the interaction region at different times. In this way, again by comparison with particle tracing simulation results, the temporal variation of E(r) was computed.

Charging of the wire is observed to commence more than 5 ps prior to the peak of the CPA_2 interaction pulse. One possible cause of such strong charging prior to the intensity peak could be the acceleration of hot electrons by the rising edge of the pulse. Autocorrelation measurements performed on Vulcan Petawatt [8] suggest that the on-target intensity 5 to 10 ps before the peak of the pulse could be a significant fraction of the peak intensity, so it is not unreasonable that the production of a hot electron population could be initiated at this time.

From the peak E-field value of 3×10^{10} V m^{-1} at the interaction time of CPA_2, the field is seen to decay in an almost linear fashion over a 15 ps timescale during which the wire discharges most probably due to the grounding effect of the target mount. Filamentary structures visible during the discharge can be attributed to the electrothermal instability induced as hot electrons returning to the wire interact with counterstreaming colder electrons [9]. Filamentation is observed to break out 10 ps after the interaction pulse has

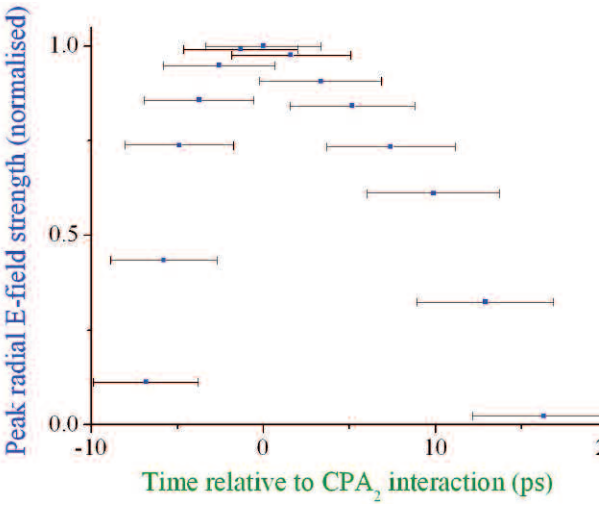

Figure 4. Electrical charging and subsequent discharging of a 100 µm Au wire irradiated by CPA_2. The horizontal error bars were determined by arbitrarily assuming the protons to suffer significant deflections during their transit of the region within 4 r_{wire} of the wire centre.

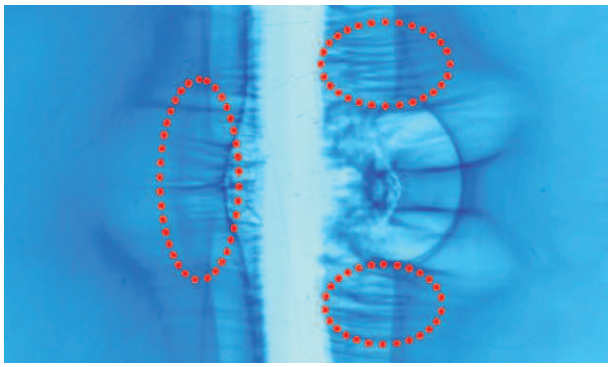

Figure 5. Filamentary structures present around the discharging wire. The laser was incident from the right. The RCF image corresponds to conditions 25 ps after the arrival of the CPA_2 interaction pulse.

arrived. The filaments expand out into vacuum with the plasma, always appearing behind the charging front. That the filaments behave in this manner and are present over relatively long timescales of tens of picoseconds supports the idea that they are quasistatic magnetic structures frozen into the expanding plasma[9,10]. At later times, the wire will proceed to explode hydrodynamically.

The data presented is similar in nature to that concerning the charge-discharge cycle of a glass microballoon under high-intensity laser irradiation[11]. The data presented here is unique in that the proton beam used to perform the probing has a much higher cutoff energy, being produced by the interaction of the mid-10^{20} W cm^{-2} pulse provided by the focused main beamline of Vulcan. As a result, both the range and resolution of the temporal picture provided here is unparalleled.

Resolution of wire charging front

Whilst the global wire charge-discharge was observed in the previous data, no information was provided on the

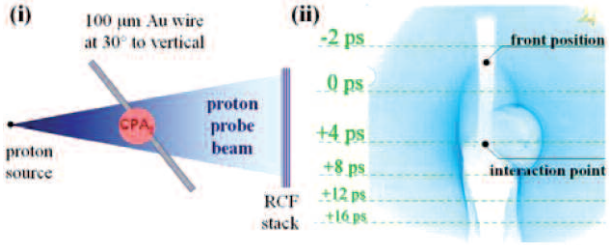

Figure 6. (i) Experimental setup for angled wire shots; (ii) schematic explaining interpretation of angled wire RCF data. The bulk of the signal on this RCF layer is formed by protons with E_p ~ 16 MeV.

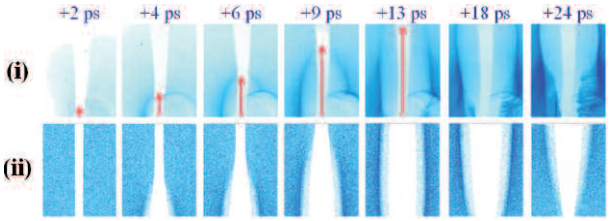

Figure 7. Experimental (i) and simulated (ii) data showing front propagation along 100 µm Au wire irradiated by CPA_2. The front motion, occurring at a velocity of close to *c*, is highlighted by the red arrows. The times shown are probing times relative to the arrival of CPA_2 for probe protons travelling past the bottom part of each image. As the wire discharges at later times, the breakout of filamentation is visible.

mechanism by which the charging fields are transferred from the region in and around the laser focus to the rest of the wire. The RCF images obtained for the CPA_2 interaction on the vertical wire are more or less discrete snapshots in time of the interaction. On one image corresponding to a time before the arrival of CPA_2, no proton deflection is visible, whilst on the adjacent RCF layer for the next probing time, just a couple of ps later, a charging front is visible along the length of the wire, so some sort of ultrafast process must occur in the intermediate time.

In the second part of the experiment, a subtle but important change was made to the setup to provide information on this intermediate time. As stated, proton imaging is basically a time of flight technique. In that case, if the interaction wire is placed at an angle to the vertical, then the protons assigned to a given RCF layer, all travelling at the same velocity, will give information on different probing times based on their angle of emission from the source. Effectively then, placing the wire at an angle to the vertical will lead to *continuous* probing of the interaction. In this way, the motion of a highly-relativistic charging front along the wire surface is resolved.

The motion of the charging front along the wire is clearly visible in the RCF images (see figure 7). Its position relative to the CPA_2 interaction point was measured as a function of time. Hence, the front was calculated to be moving at a velocity ~ *c*. The radial field profiles computed earlier in the CPA_2 interaction with the vertical wire were fed into the particle tracer for the angled wire case. The

temporal variation of field magnitude was also taken account of in the simulations. Once more, there was good agreement between the experimental and simulated data. Note how the transition of the wire from its uncharged to its charged state is visible on a single layer due to the range of times associated to different points along the wire. At late times after the interaction, the wire was observed to discharge just as in the case of the vertical wire. The onset of strong filamentation is once again visible from +10 ps onwards.

Conclusions

The present work shows with unprecedented detail the electrical charging and discharging of a metallic wire that has been irradiated at ultrahigh intensity. Moreover, the propagation of a highly-relativistic charging front moving at c along the wire was resolved before the filamentary structures indicative of discharge were observed.

The interpretation and modelling of the data is currently in progress, however some possible scenarios can be highlighted. In the CPA_2 interaction with the wire, the most energetic laser-accelerated electrons will be lost to vacuum. After a short time, the wire will be left with a large net positive charge, drawing a cold return current from the numerous electrons of the bulk target. As a result of the Coulomb forces at work, this redistribution of charge may in turn lead to a kind of *domino effect* both up and down the wire which could be interpreted as a positive current flowing away from the laser focus. This is a possible framework for the production of the observed highly transient electromagnetic pulse propagating along the wire at *c* which rises and decays over a 25 ps time window.

Furthermore, some of the hot electrons excited in the interaction region will return to the wire via the fountain effect. Those with some component of their velocity along the wire axis will invariably move along the wire in either direction away from the region of the laser focus. That the hot electrons can be confined to the region around the target in this way is demonstrated by the simulation results of figure 8. Only along the wire may $\boldsymbol{j}_{hot} = -\boldsymbol{j}_{cold}$ be satisfied [1].

Further work is required, however, to understand more about the mechanism by which these fields are transported along the length of the wire. In particular, the processes at work inside the wire and the role of magnetic fields remain uncertain.

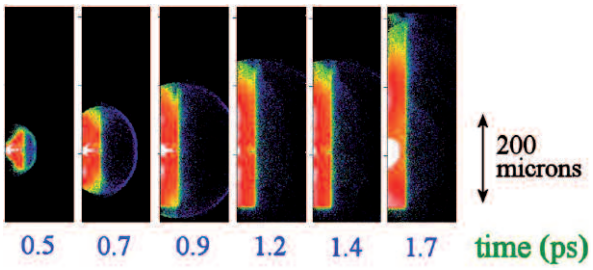

Figure 8. LSP simulation detailing incidence of an intense, short-pulse IR laser on a metallic slab. The vertical slab occupies the left quarter of the image. A hot electron population, visible in red, is propagated away from the laser focus both upwards and downwards, transverse to the laser axis, at the speed of light. Note the confinement of the electron currents to the region around the slab.

Acknowledgements

The author would like to acknowledge the invaluable help of the staff of the Central Laser Facility.

References

1. R. R. Freeman *et al.*, *Fus. Sci. Tech.* **49**, 297 (2006).
2. R. Gibbon, *Short Pulse Laser Interactions with Matter*, Imperial College Press (2005).
3. P. Mora, *Phys. Rev. Lett.* **90**, 185002 (2003).
4. M. Borghesi *et al.*, *Fus. Sci. Tech.* **49**, 412 (2006) and references therein.
5. L. Romagnani *et al.*, *Phys. Rev. Lett.* **95**, 195001 (2005).
6. N. V. Klassen *et al.*, *Med. Phys.* **24**, 1924 (1997).
7. C. N. Danson *et al.*, *Nucl. Fusion* **44**, S239 (2004).
8. C. Hernandez-Gomez *et al.*, CLF Annual Report 2004/2005, page 200 (2005).
9. M. G. Haines, *Phys. Rev. Lett.* **47**, 917 (1981).
10. F. Beg *et al.*, *Phys. Rev. Lett.* **92**, 095001 (2004).
11. M. Borghesi *et al.*, *Appl. Phys. Lett.* **82**, 1529 (2003).